Article

Chinese Science Bulletin

Progress of Projects Supported by NSFC
Oceanology

November 2011 Vol.56 No.33: 3558–3565
doi: 10.1007/s11434-011-4685-7

Turbidite deposition in the southern South China Sea during the last glacial: Evidence from grain-size and major elements records

ZHAO YuLong[1,2*], LIU ZhiFei[1], COLIN Christophe[2], XIE Xin[1] & WU Qiong[1,2]

[1] *State Key Laboratory of Marine Geology, Tongji University, Shanghai 200092, China;*
[2] *Laboratoire des Interactions et Dynamique des Environnements de Surface (IDES), UMR 8148 CNRS-Université Paris-Sud 11, Orsay 91405, France*

Received May 11, 2011; accepted July 6, 2011; published online August 30, 2011

High-resolution grain size and major element geochemical measurements were performed on the marine sediments of Core MD05-2895 to help understand the formation of turbidite sequences. Grain-size results show that these turbidite sediments contain more coarse sediment grains than normal marls. The coarse sediment grains are mostly derived from relict sediments on the Sunda Shelf. Relict sediments are composed mainly of quartz, feldspar, tephra and a few titaniferous or ferruginous heavy minerals. Corresponding to the concentration of these minerals, increases in Si/Al, K/Al, Ti/Al and Fe/Al ratios are observed in the turbidite layers. As all the observed turbidite sequences were deposited during the last glacial, the occurrence of these turbidity events is implied to be closely related to instabilities in sea-level-induced sediment supply. We suggest that deposition of sediment particles from a single turbidity current is usually controlled by a counterbalance between gravity and buoyancy, with the interaction of individual grains being of minor importance.

Southern South China Sea, last glacial, turbidite, grain-size analyses, XRF Core Scanner

Citation: Zhao Y L, Liu Z F, Colin C, et al. Turbidite deposition in the southern South China Sea during the last glacial: Evidence from grain-size and major elements records. Chinese Sci Bull, 2011, 56: 3558–3565, doi: 10.1007/s11434-011-4685-7

Turbidity currents are probably the most common deep-sea gravity-driven currents in the world's oceans. The occurrence of turbidity activities is usually destructive to submarine cables and oceanographic observation apparatus. Turbidite sequences in sedimentary records are adopted widely to interpret the emergence of abyssal valleys and submarine fans [1–3], the formation and preservation of offshore hydrocarbons [4,5], and even as indicators of paleoclimate [6–8]. Therefore, the formation mechanisms of turbidites are of broad interest to sedimentologists from a wide range of disciplines. In the last decades, geophysical exploration of the most famous deep-sea turbidite systems, such as the Nile deep-sea fan, the Mississippi fan, and the Amazon fan, has largely enhanced our knowledge about the mechanisms and dynamics of large-scale turbidite system formation [9–13]. However, sequences in such large-scale turbidite systems are often well mixed with each other, such that the separation of a single turbidite layer from the sediments of a large-scale turbidite system is almost unlikely. Recently, laboratory experiments [14,15] and numerical modeling [16] have been introduced to investigate the formation of a small-scale single turbidite layer. Laboratory experiments and numerical modeling, nevertheless, cannot reproduce natural marine environments, given their spatial extent and duration. On the other hand, real-time observation, albeit the most direct way to study naturally occurring turbidity flows, is almost impossible because the triggering of turbidity activities is difficult to predict and the resulting flows are usually destructive. Therefore, the most feasible way to study the formation of single turbidite layers is to investigate well-preserved turbidite sequences in marine sediments. Focus is on the recognition of turbidites, as well-preserved turbidite sequences are very rare in marine sediments.

The Sunda Shelf, which extends to more than 800 km at

*Corresponding author (email: yeoloon@gmail.com)

its widest, is one of the broadest continental shelves in the world [17]. The land-sea configuration of the Sunda Shelf was therefore dramatically influenced by fluctuations of sea level during the late Pleistocene [18]. During sea-level lowstands, by virtue of the extensive drainage system developed on the Sunda shelf, great masses of sediments were delivered directly to the edge of the continental slope. These sediments were highly unstable, which supported the instigation of turbidity events. In this study, terrigenous grain-size and major element geochemical results of several turbidite layers in the southern South China Sea (SCS) are presented to investigate the formation of turbidite sequences in marine sediments.

1 Materials and methods

Core MD05-2895 (07°02.25′N, 111°33.11′E, water depth 1982 m, Figure 1) was collected at the base of Sunda Slope

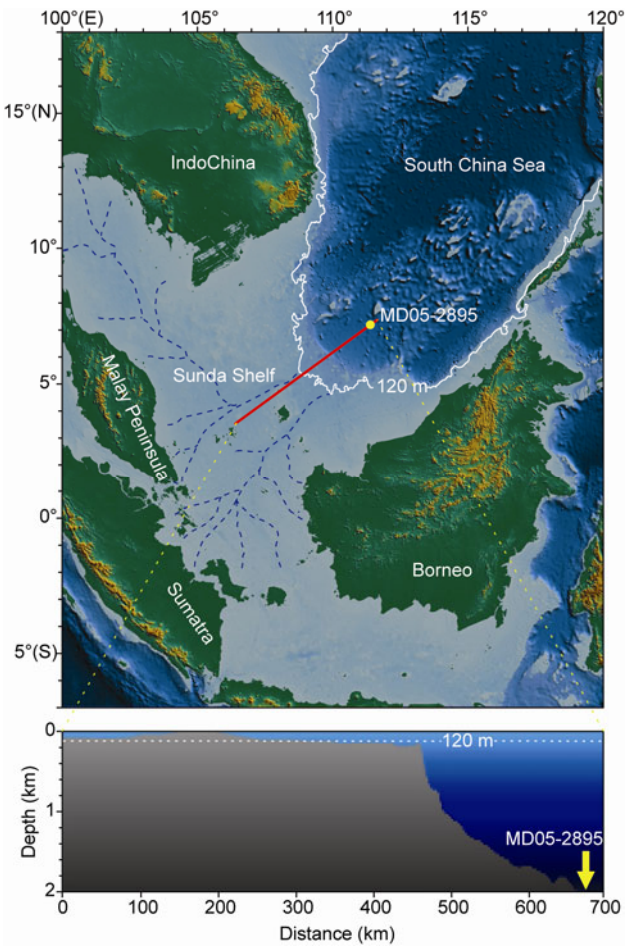

Figure 1 Sitemap of Core MD05-2895. Bathymetry of the southern SCS is illustrated by variation of color. The white solid line shows the shoreline during the last glacial maximum. Dashed lines in blue show paleo-rivers developed on the Sunda Shelf during the last glacial. The red solid line presents the position of the topographic profile below.

during the MD147–"Marco Polo" Cruise in September 2005 [19]. Its position is coincident with box core MD05- 2894 collected during the same cruise [19]. The sediment of Core MD05-2895 consists mostly of olive-gray clay. Five layers of coarse sediment were recorded between sub-seafloor depths of 15 and 30 m, with thicknesses varying between 40 and 160 cm [19]. At the bottom of these coarse sediment layers, unconformity contacts as well as scour marks are visually observable. Laser grain-size and XRF Core Scanner geochemical analyses were performed on the 15–30 m interval of Core MD05-2895 to explore the sedimentological and geochemical compositions of these coarse layers. Surface features of the coarse sediments were analyzed using an XL-30 environmental scanning electron microscope (ESEM) at the State Key Laboratory of Marine Geology, Tongji University. The Energy Dispersive Spectrometer (EDS) system affiliated with the SEM was adopted to detect the geochemical compositions of sediment grains.

Estimates of the ages of the coarse sediment layers are based on two AMS ^{14}C age points. The test is performed on species of planktonic foraminifer *Orbulina universa*. Calibrated ages of the two samples, at depths of 23.05–23.10 m and 29.60–29.50 m, were established to be 33028±270 yr and 38788±419 yr, respectively. Given that sediments at 3.68 m of Core MD05-2894 (the equivalent of 5.44 m in Core MD05-2895) were dated in earlier work to be about 17000 yr [20], we can conclude that the whole 15–30 m interval was deposited during the last glacial period (MIS 2-4).

Laser grain-size measurements of carbonate-free sediments were carried out on a Coulter LS-230 Laser Particle Size Analyzer at the State Key Laboratory of Marine Geology, Tongji University. The depth interval for the grain-size analyses was set to 2 cm, and a total of 709 samples were analyzed. It has previously been reported that biogenic opal in pelagic deposits may significantly influence both the siliciclastic grain-size distribution and bulk sediment XRF measurements [21]. Therefore, ten samples from different layers were measured using the molybdate blue spectrophotometric method [22] to test the opal content in the sediments. Results show that the opal contents in all ten samples are less than 2%. The presence of opal on grain-size and geochemical measurement is thus considered to have negligible influence in Core MD05-2895.

Major element geochemical analyses were performed directly on the surface of split cores at 1 cm intervals using an Avaatech XRF Core Scanner at the State Key Laboratory of Marine Geology, Tongji University. The surfaces of the core sections were covered with a 4 μm thick Ultralene® foil to avoid contamination of the XRF measurement unit and desiccation of the sediment. Measurements were performed at settings of 10 kV and 500 mA to obtain the intensities of elements from Al to Fe. Before covering with the foil, digital photos of the core sections were taken using a 3 CCD (Charge Coupled Device) line scan camera affiliated to the XRF Core Scanner.

2 Results

2.1 Siliciclastic grain size

Median grain size values in the "normal" marls of Core MD05-2895 are shown to vary in the range of 5–10 μm. The marl sediments are dominated by clay (< 4 μm) and silt (4–63 μm), with the contents of each fraction varying from 40%–60% (Figure 2). In regard to the coarse sediment layers, the grain-size distribution of the marl sediments constitutes "background" values. The coarse sediment layers are simply denoted downwards by labels T1 to T5 (Figure 2). The median grain size shifts abruptly to 50–70 μm at the bottom of the coarse sediment layers and then gradually decreases upward to the "background" median values, forming a typical normally-graded sequence (Figure 2). The sediment grain size composition in the coarse layers differs greatly from that in the marls – the clay fraction is drastically decreased to ~10% in the coarse layers, and the silt fraction is decreased slightly to 30%–40%. The sand (> 63 μm) fraction in the coarse units can reach ~50%, compared with negligible amounts in the marls.

2.2 Geochemical results

The relative abundance of each element measured by the XRF Core Scanner is reported versus total counts, which is proportional to the chemical concentration of the specific element. Consideration of elements with average total counts less than 1000 are excluded to diminish errors. Owing to its conservative behavior in weathering profiles, Al is employed as a normalization parameter to assess the relative degrees of enrichment or depletion of specific elements and to eliminate dilution from carbonate and organic fractions [23]. Ratios of elements Si, K, Ti, and Fe versus Al are displayed in Figure 3. Variations of Si/Al, K/Al, Ti/Al, and Fe/Al are observed to be closely related to changes in particle grain size. The values of these ratios increase rapidly at the bottom of the coarse sediment layers and then gradually decrease to the values expected for "normal" marls (Figure 3).

2.3 Electron photomicrography results

Prior to the SEM with EDS analyses, raw samples were rinsed over a 37.5 μm mesh sieve and cleaned thoroughly to eliminate any particles attached to the surface of grains. Photomicrography of the sample at 18.48 m depth (in T2) is displayed in Figure 4. Sediments in the coarse fractions generally consist of K-feldspar, quartz, mica, tephra and a few heavy mineral grains (Figure 4(a)). Grains of K-feldspar are moderately kaolinized (Figure 4(b)), indicating that they have undergone severe chemical denudation. Elongated vesicles as well as fluidal textures are observed in the structure of tephra (Figure 4(c)), implying that the sources

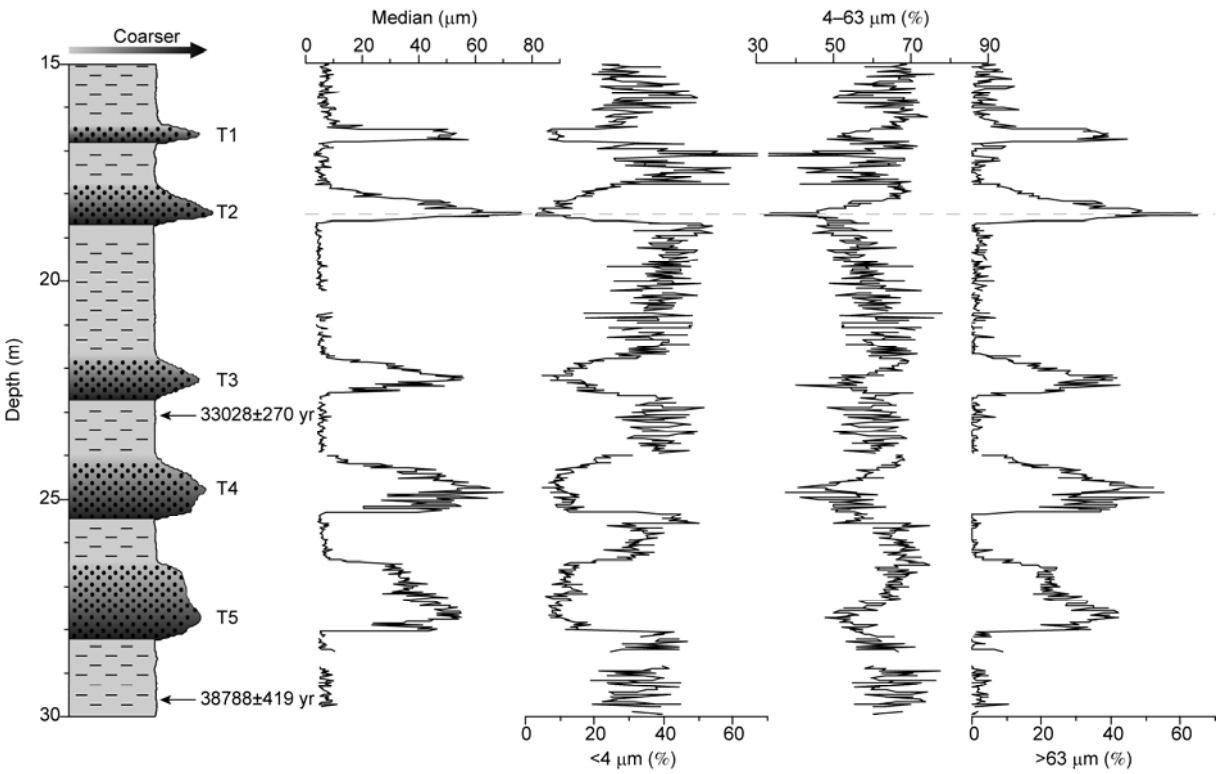

Figure 2 Down core variation of terrigenous grain size in Core MD05-2895. The coarse sediment layers are denoted by T1 to T5. Arrows beside the lithological log indicate the depth of samples which are AMS ^{14}C dated. Gray dashed line shows the position of sample displayed in Figure 4.

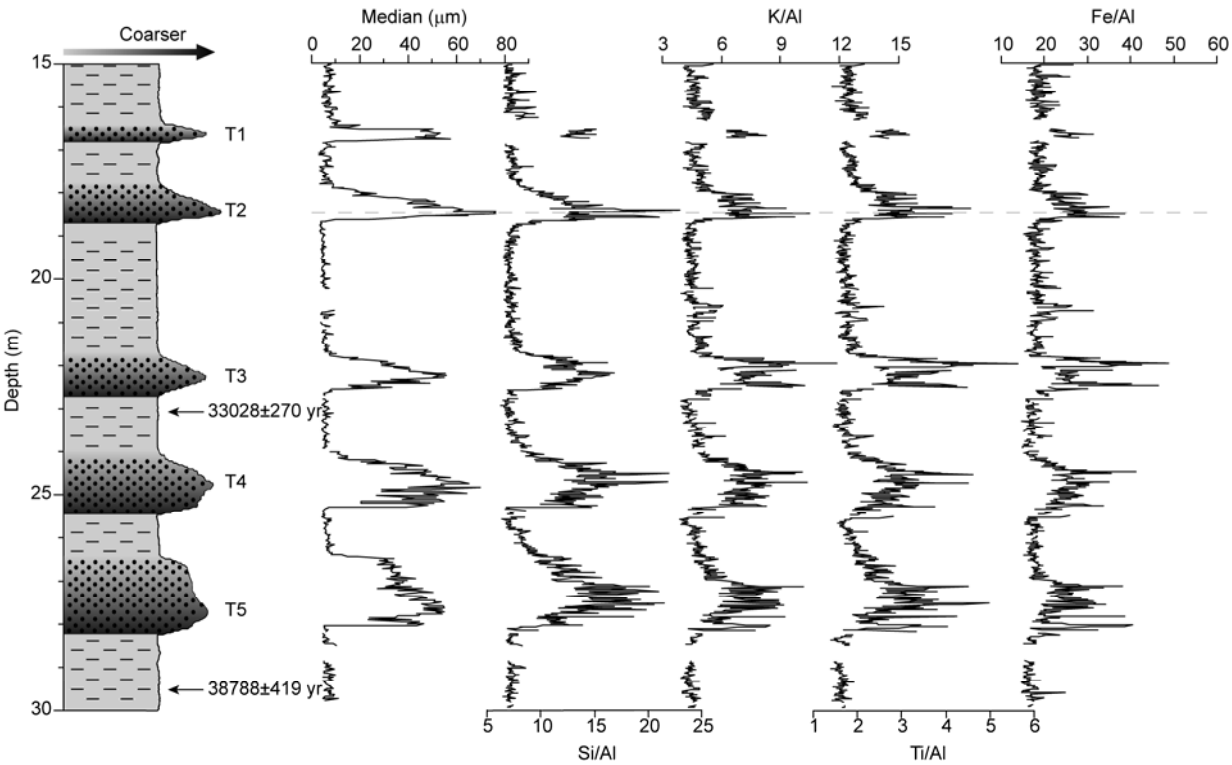

Figure 3 Down core variation of major element ratios in Core MD05-2895. The coarse sediment layers are denoted by T1 to T5. Arrows beside the lithological log indicate the depth of samples which are AMS ^{14}C dated. Gray dashed line shows the position of sample displayed in Figure 4.

of volcanic ashes in Core MD05-2895 are closely linked to felsic magma. Fractures are observed on some grains of quartz (Figure 4(d)).

3 Discussion

3.1 Sources of particles in the coarse sediment layers

Generally speaking, most coarse sediment grains are unlikely to reach the lower continental shelf under normal hydrodynamic conditions. However, during sea-level lowstands when estuaries extend further seaward, great masses of sediments can be transported to the lower shelf, even to the edge of continental slope. When sea-level rises again, these coarse relict sediments are left on the lower shelf [24]. The relict sediments, which are usually highly unstable, can easily be transported to the deep-sea basin by gravity currents. Two sources of terrigenous sediments are recognized for the southern SCS – the Sunda Shelf and Borneo [25]. However, during the last glacial period, terrigenous sediments at this site were mostly provided by the Sunda Shelf while sediments from Borneo were of minor importance [26]. Provided that the grains of tephra and quartz observed in the coarse fraction of Core MD05-2895 respectively have similar morphological and geochemical features with tephra derived from Sumatra [27,28] and quartz in the relict sediments of the Sunda Shelf [29,30], we can assume that the coarse sediments have a common provenance with the relict sediments on the Sunda shelf, probably as a result of their redistribution.

3.2 Formation of the coarse sediment layers

Sediments transported to deep-sea basins by rivers are usually finer in grain size, whereas silty to sandy grains in marine sediments are generally considered to originate from either eolian inputs or gravity current activities. Dominated by a hot and humid tropical climate and densely covered by vegetation, negligible amounts of dust are generated on the lands adjacent to the southern SCS. Additionally, eolian input is unlikely to explain why the coarse sediment layers in Core MD05-2895 are normally graded and unconformable with underlying marls. These coarse sediment layers are therefore likely to have been formed by submarine gravity currents.

Turbidity currents are one of the most common types of gravity current, the occurrence of which has great significance to the sedimentology of marginal seas. For sedimentologists, however, recognition of turbidites is usually problematic, because they are rarely fully preserved in marine sediments. In 1962, Bouma introduced a model sedimentary sequence, referred to since as a “Bouma sequence”, to represent the ideal sedimentary sequence formed by turbidity currents [31]. However, complete Bouma sequences are rarely observed in marine sediments, and fragments, despite widely being applied as a criterion of turbidite sequences,

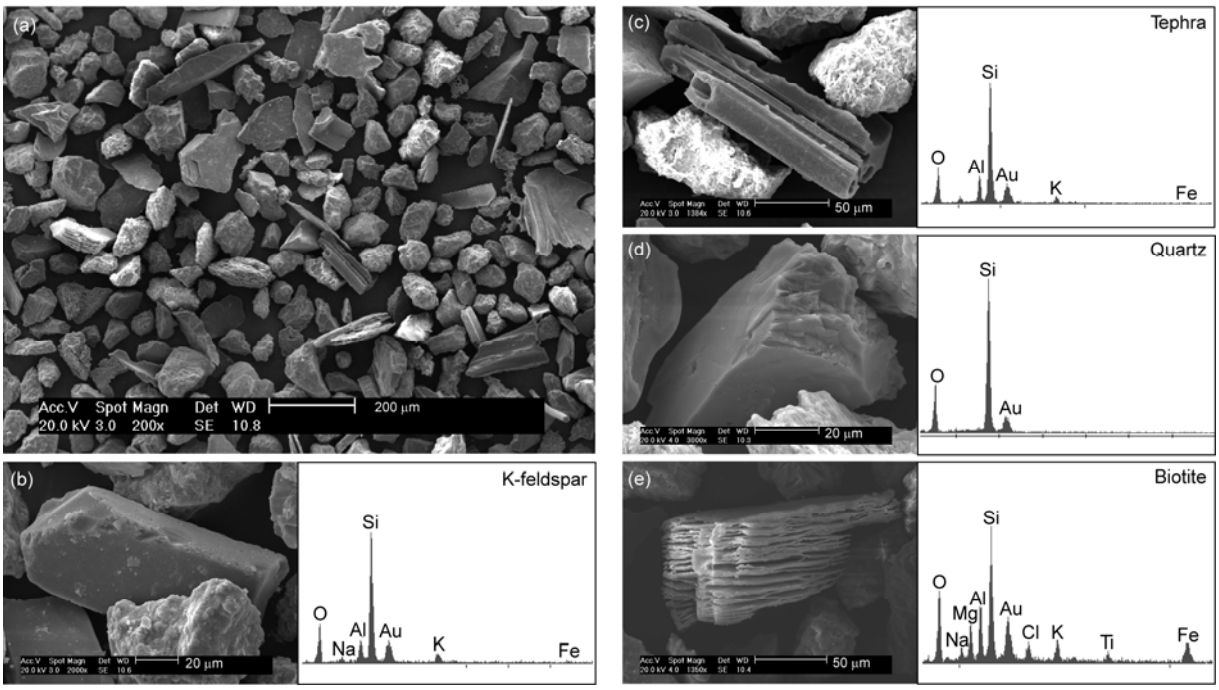

Figure 4 SEM photos of coarse sediment grains (>37.5 μm) in turbidite. The sample is taken from T2 at a depth of 18.48 m. The affiliated spectra show energy-dispersive spectroscopy (EDS) of respective grains. (a) Panorama of grains; (b) K-feldspar; (c) tephra; (d) quartz; (e) biotite.

are actually ambiguous in proving a formation mechanism. Some part of a Bouma sequence is also capable of being formed in other sedimentary processes [32]. Based on visual observation and petrographic description of more than 6000 m of sediment cores from all around the world ocean, Shanmugan [32] found that an overwhelming majority of turbidite sequences possess an indicative fining-upward normally-graded layering. As a result, he recommended using normally-graded coarse sediment layers as an indicator of turbidite sequences [32]. Consequently, formation of the coarse sediment layers observed in Core MD05-2895 are attributed to turbidity currents, as they fit the exact features of turbidites suggested by Shanmugan [32].

The Sunda Shelf, which extends up to more than 800 km at its widest, is characterized by an extremely low average gradient of merely 0.03°. A less than 10 m sea-level change could probably lead to a transgression or regression of the shoreline of several tens of kilometers. Relative to the Holocene [33], global sea-level underwent frequent and rapid changes during the last glacial period, which had a great impact on sediment supply to the southern SCS [18]. Note that all turbidity events observed in this study occurred during the last glacial, we therefore infer that the formation of the turbidite layers in Core MD05-2895 is closely related to a sea-level-induced sediment supply instability. Nevertheless, considering that sea-level changes usually occur on a decadal to centennial scale, whereas turbidity events are almost instantaneous, sea-level-induced sediment supply instabilities are unlikely to have been the direct trigger of turbidity flows. Generally speaking, deep-sea turbidity events can be triggered by some catastrophic tectonic (e.g. a volcanic eruption or earthquake) or extreme meteorological (e.g. rainstorm or typhoon) events. However, turbidity flows are more likely in an environment with an unstable, rather than stable, sediment supply, assuming that the intensity of the triggering is at the same level. Therefore, we suggest that even though instabilities in sea-level-induced sediment supply do not directly trigger turbidity events, they do increase the probability of turbidity events.

3.3 Depositional mechanism of grains in turbidity currents

Owing to the uncertainty of hydrodynamic and support mechanisms, there has long been a controversy involving how particles are deposited from turbidity currents [34]. Presently, two contradictory opinions are considered. One view, Model 1, holds that particles are deposited *en masse* from turbidity currents [35–37]. They suggest that as time passes, the basal part of the currents becomes denser until the buoyancy is reduced to the point where it is not sufficient to support the flow. Particles then deposit almost instantaneously out from the current [35–37]. In Model 1, the current, especially the basal part, is largely supported by grain-to-grain interaction [35–37]. A second opinion, Model 2, is that turbidity currents are mostly supported by turbulent suspension, and deposition of particles occurs grain-by-grain by progressive aggradation [38,39]. In Model 2, depo-

sition of a single particle is controlled by the counterbalance between buoyancy and gravity, and interaction between grains is considered negligible [38,39]. As for Model 1, the whole mass of sediment grains in the basal part acts as an ensemble, and movement of a single grain is mostly decided by grain-to-grain interaction [35–37]. Grain-size distribu-

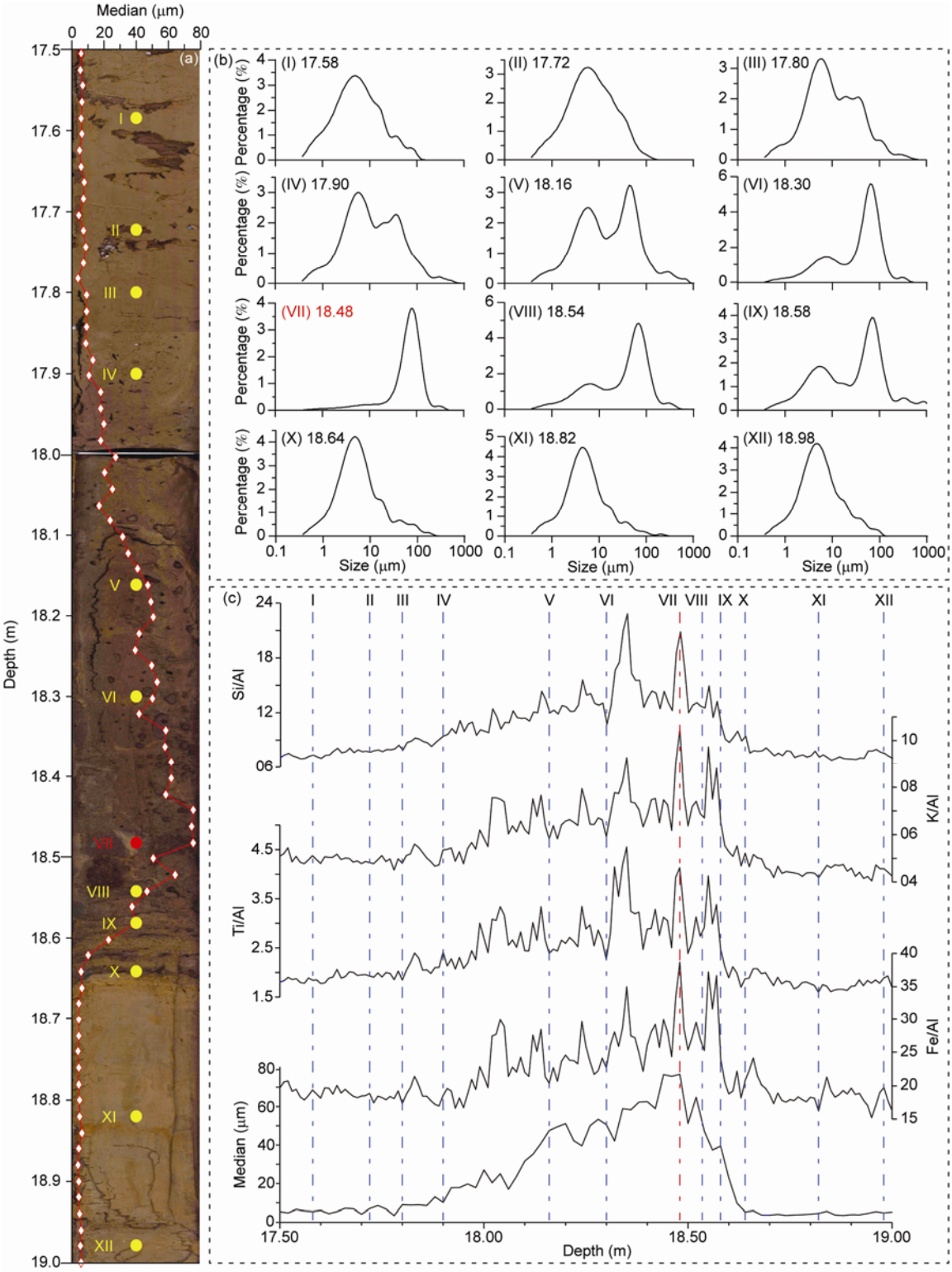

Figure 5 A compilation of grain-size and geochemical variation of T2. (a) Line scan photograph plotted with grain-size median values; yellow and red (the position of sample displayed in Figure 4) dots indicate the depths of grain-size frequency curves shown in (b). (b) Grain-size frequency curves of samples at specific depths. (c) Variations of major element ratios. Dashed blue line indicates the depths of grain-size frequency curves shown in (b).

tions of sequences formed by these two model processes are different from each other. Sequences formed by Model 1 generally have a sharp contact with bilateral marls, but the sediment within the sequence is badly sorted or unsorted [35–37]. In some large-scale turbidity activities, the *en masse* deposition may have occurred several times, forming staircase-like fining-upward sequences [35–37]. In contrast, sequences formed by Model 2 are usually well sorted, with particles forming a fining-upward normal-graded layer [38,39]. The bottoms of the sequences formed by Model 2 contact sharply with the underlying marls, whereas the tops of the sequences are continuous with the marls [38,39].

To better understand the formation of a turbidite, layer T2 is broken down into its constituent parts to observe the internal variation of terrigenous grain-sizes and geochemical make-up. As seen from the digital photos, there is a clear unconformity between the bottom of T2 and the underlying sediments (Figure 5(a)). The median grain-size values increase rapidly to a maximum within a depth interval of only 16 cm (18.64–18.48 m), whereas it takes 58 cm (18.48–17.90 m) for the median values to decrease to the "background" values (Figure 5(a)). An increase of median values usually corresponds to an increase in the coarser fraction (Figure 5(b), VII–X), whereas a decrease of median values corresponds to an increase in the finer fraction (Figure 5(b), II–VI). Element ratios (Si/Al, K/Al, Ti/Al and Fe/Al) generally follow the variation of median grain-size values, though more variable (Figure 5(c)). Si, K, Ti and Fe in the turbidite are correlated respectively to quartz, feldspar, and Ti- or Fe-bearing heavy minerals. These minerals are generally larger in grain size and denser than the clay minerals (the main source of Al in marine sediments). Therefore, the variation of Si/Al, K/Al, Ti/Al and Fe/Al values in T2 actually reflects the intensity of sorting in the turbidite. Combining the grain-size and geochemical results, we can conclude that the turbidite sequences in Core MD05-2895 are formed by the processes of Model 2 (i.e. grain-by-grain progressive aggradation).

4 Conclusions

In this study, the first high-resolution grain-size and geochemical results of deep-sea turbidites from the southern SCS are presented. We arrive at the following three conclusions.

(1) Five turbidite layers are observed in Core MD05-2895. In comparison to the "normal" marls in the core, the proportion of clay is drastically decreased in the turbidites, whereas the proportion of sand is greatly increased. Median grain-size values present a rapid increase and then a gradual decrease in the turbidite sequences, forming typical fining-upward normally-graded sequences. Coarser grains (>37.5 μm) in the turbidite are observed to be mineralogically composed of quartz, K-feldspar, Ti- and Fe-bearing heavy minerals. Corresponding to the concentration of these minerals, an increase in Si/Al, K/Al, Ti/Al and Fe/Al ratios is observed in the turbidite layers.

(2) Coarse mineral grains in Core MD05-2895 are derived mostly from the redistribution of relict sediments on the Sunda Shelf. The formation of the turbidite layers is closely related to sea-level-induced sediment supply instabilities. However, the instability of sediment supply is unlikely to be the direct trigger of turbidity flows. Rather, the influence of sediment supply instabilities on turbidity events results from the fact that turbidity events are more easily triggered if the sediment supply is unstable.

(3) The deposition of sediment particles in turbidity currents is controlled by the counterbalance between gravity and buoyancy. The interaction between grains is of minor importance to the deposition of sediments. Sorted by grain-size and density, sediment grains deposited from a turbidity current will form a fining-upward normally-graded sequence.

The authors give thanks to Li Xiajing, Huang Enqing, and Xia Peifen for their assistance during sample preparation. Dr. Thomas Ritcher from the NIOZ (the Royal Netherlands Institute for Sea Research) is appreciated for the helpful discussion. Andrew Gorman is thanked for polishing the English language. Acknowledgment is also expressed to all the participants on board of the R/V Marion Dufresne during the MD147–"Marco Polo" Cruise. This work was supported by the National Natural Science Foundation of China (40925008, 40876024 and 40776027), the National Basic Research Program of China (2007CB815906) and the Program of Shanghai Subject Chief Scientist (10XD1406300).

1 Shanmugam G, Moiola R J. Submarine fans: Characteristics, models, classification, and reservoir potential. Earth-Sci Rev, 1988, 24: 383–428
2 Piper D J W, Deptuck M. Fined-grained turbidites of the Amazon Fan: facies characterization and interpretation. In: Flood R D, Piper D J W, Klaus A, et al., eds. Proceedings of the Ocean Drilling Program-Scientific Results 155. Texas, ODP College Station, 1997. 79–108
3 Zuff G G, Normark W R, Serra F, et al. Turbidite megabeds in an oceanic rift valley recording Jökulhlaups of late Pleistocene glacial lakes of the western United States. J Geol, 2000, 108: 253–274
4 Liu X B, Wan X Q, Lin J C, et al. Continental turbidite deposition system and hydrocarbon (in Chinese). Acta Geosci Sin, 2003, 24: 61–66
5 Wang C W, Chen H H, Chen C, et al. The identification of the Baiyun deep-water fan and the key factors of petroleum accumulation in Pearl River Mouth Basin (in Chinese). J Southwest Petrol Univ, 2007, 29: 12–16
6 Prins M A, Postma G. Effects of climate, sea-level, and tectonics unraveled for last deglaciation turbidite records of the Arabian Sea. Geology, 2000, 28: 375–378
7 Weber M E, Wiedicke-Hombach M, Kudrass H R, et al. Bengal Fan sediment transport activity and response to climate forcing inferred from sediment physical properties. Sediment Geol, 2003, 155: 361–381
8 Weltje G J, De Boer P L. Astronomically induced paleoclimatic oscillations reflected in Pliocene turbidite deposits of Corfu (Greece): Implications for the interpretation of higher order cyclicity in fossil turbidite systems. Geology, 1993, 21: 307–310
9 Maldonado A, Stanley D J. The Nile Cone: Submarine fan development by cyclic sedimentation. Mar Geol, 1976, 20: 27–35; 39–40
10 Loncke L, Gaullier V, Droz L, et al. Multi-scale slope instabilities along the Nile deep-sea fan, Egyptian margin: A general overview. Mar Petrol Geol, 2009, 26: 633–646

11 Pirmez C, Imran J. Reconstruction of turbidity currents in Amazon Channel. Mar Petrol Geol, 2003, 20: 823–849
12 Kastens K A, Shor A N. Evolution of a channel meander on the Mississippi deep-sea fan. Mar Geol, 1986, 71: 165–175
13 Shanmugam G, Moiola R J, McPherson J G, et al. Comparison of turbidite facies associations in modern passive-margin Mississippi fan with ancient active-margin fans. Sediment Geol, 1988, 58: 63–77
14 Amy L A, Peakall J, Talling P J. Density- and viscosity-stratified gravity currents: Insight from laboratory experiments and implications for submarine flow deposits. Sediment Geol, 2005, 179: 5–29
15 Hallworth M A, Huppert H E. Abrupt transitions in high-concentration, particle-driven gravity currents. Phys Fluids, 1998, 10: 1083–1087
16 Felix M. Flow structure of turbidity currents. Sedimentology, 2002, 49: 397–419
17 Steinke S, Kienast M, Hanebuth T J. On the significance of sea-level variations and shelf paleo-morphology in governing sedimentation in the southern South China Sea during the last deglaciation. Mar Geol, 2003, 201: 179–206
18 Hanebuth T J J, Stattegger K, Grootes P M. Rapid flooding of the Sunda shelf: A late-glacial sea-level record. Science, 2000, 288: 1033–1035
19 Laj C, Wang P, Balut Y. Les rapports de campagnes à la mer à bord du "Marion Dufresne": MD147/MARCO POLO-IMAGES XII. Brest: Institut Polaire Français (IPEV), 2005
20 An Y, Jian Z M. Pulleniatina Minimum Event during the last deglaciation in the southern South China Sea. Chinese Sci Bull, 2009, 54: 4514–4519
21 Xie X, Zheng H B, Chen G C, et al. Pretreatment method of grain size measurement of marine sediments in paleoenvironment research (in Chinese). Acta Sedimentol Sin, 2007, 25: 684–692
22 Mortlock R A, Froelich P N. A simple method for the rapid determination of biogenic opal in the pelagic marine sediments. Deep Sea Res Part A: Oceanogr Res Paper, 1989, 36: 1415–1426
23 Calvert S E, Pedersen T F. Elemental proxies for palaeoclimatic and palaeoceanographic variability in marine sediments: Interpretation and application. In: Hillaire-Marcel C, De Vernal A, eds. Proxies in Late Cenozoic Paleoceanography. Amsterdam: Elsevier Publishing, 2007. 567–644
24 McManus D A. Modern versus relict sediment on the continental shelf. Geol Soc Am Bull, 1975, 86: 1154–1160
25 Steinke S, Hanebuth T J J, Vogt C, et al. Sea level induced variations in clay mineral composition in the southwestern South China Sea over the past 17000 a. Mar Geol, 2008, 250: 199–210
26 Wang H. Clay mineralogy and element geochemistry in the southern South China Sea since the last glacial maximum and their paleoenvironmental implication (in Chinese). Master's Thesis. Shanghai: Tongji University, 2011. 41–52
27 Song S R, Chen C-H, Lee M Y, et al. Newly discovered eastern dispersal of the youngest Toba Tuff. Mar Geol, 2000, 167: 303–312
28 Liu Z, Colin C, Trentesaux A. Major element geochemistry of glass shards and minerals of the Youngest Toba Tephra in the southwestern South China Sea. J Asian Earth Sci, 2006, 27: 99–107
29 Wu S, Luo Y. The relict sediments in the south shelf of South China Sea (in Chinese). J Tropical Oceanogr, 1994, 13: 47–53
30 Wu S, Wong H K, Luo Y, et al. Distribution and origin of sediments on the northern Sunda Shelf, South China Sea. Chin J Oceanol Limnol, 1999, 17: 28–40
31 Bouma, A H. Sedimentology of Some Flysch Deposits: A Graphic Approach to Facies Interoretation. Amsterdam: Elsevier Publishing, 1962
32 Shanmugan G. The Bouma Sequence and the turbidite mind set. Earth-Sci Rev, 1997, 42: 201–229
33 Peltier W R. On eustatic sea level history: Last Glacial Maximum to Holocene. Quat Sci Rev, 2002, 21: 377–396
34 Kneller B, Buckee C. The structure and fluid mechanics of turbidity currents: A review of some recent studies and their geological implications. Sedimentology, 2000, 47(Suppl 1): 62–94
35 Shanmugam G. High-density turbidity currents: are they sandy debris flow? J Sediment Res, 1996, 66: 2–10
36 Wilson C J N. Emplacement of Taupo ignimbrite. Nature, 1997, 385: 306–307
37 Mulder T, Savoye B, Syvitski J P M. Numerical modelling of a mid-sized gravity flow: The 1979 Nice turbidity current (dynamics, processes, sediment budget and seafloor impact). Sedimentology, 1997, 44: 305–326
38 Kneller B, Branney M. Sustained high density turbidity current and the deposition of thick massive sands. Sedimentology, 1995, 42: 607–616
39 Hiscott R N, Pickering K T, Bouma A H, et al. Basin-floor fans in the North Sea: Sequence stratigraphic models vs. sedimentary facies: discussion. Am Assoc Petrol Geol Bull, 1997, 61: 662–665